

Discriminative dictionary learning for local LV wall motion classification in cardiac MRI

J.J. Mantilla, J.L. Paredes, J.-J. Bellanger, Erwan Donal, Christophe Leclercq, M. Garreau

▶ **To cite this version:**

J.J. Mantilla, J.L. Paredes, J.-J. Bellanger, Erwan Donal, Christophe Leclercq, et al.. Discriminative dictionary learning for local LV wall motion classification in cardiac MRI. Expert Systems with Applications, 2019, 129, pp.286-295. 10.1016/j.eswa.2019.04.010 . hal-02121140

HAL Id: hal-02121140

https://univ-rennes.hal.science/hal-02121140

Submitted on 22 Oct 2021

HAL is a multi-disciplinary open access archive for the deposit and dissemination of scientific research documents, whether they are published or not. The documents may come from teaching and research institutions in France or abroad, or from public or private research centers.

L'archive ouverte pluridisciplinaire **HAL**, est destinée au dépôt et à la diffusion de documents scientifiques de niveau recherche, publiés ou non, émanant des établissements d'enseignement et de recherche français ou étrangers, des laboratoires publics ou privés.



Distributed under a Creative Commons Attribution - NonCommercial 4.0 International License

Version of Record: https://www.sciencedirect.com/science/article/pii/S0957417419302404
Manuscript_a6270ba273ecd46cb7a482c275ebf5bd

Discriminative dictionary learning for local LV wall motion classification in cardiac MRI

Juan José Mantilla[a,b], José Luis Paredes[b], Jean-Jacques Bellanger[a], Erwan Donal[a], Christophe Leclercq[a], Mireille Garreau[a,*]

[a] *Univ Rennes, CHU Rennes, Inserm, LTSI UMR 1099, F-35000 Rennes, France*
[b] *Center for Biomedical Engineering and Telemedicine (CIByTEL). Universidad de Los Andes. Mérida, Venezuela*

Abstract

The characterization of cardiac function is of high clinical interest for early diagnosis and better patient follow-up in cardiovascular diseases. A large number of cardiac image analysis methods and more precisely in cine-Magnetic Resonance Imaging (MRI) have been proposed to quantify both shape and motion parameters. However, the first major problem to address lies in the cardiac image segmentation that is most often needed to extract the myocardium before any other process such as motion tracking, or registration. Moreover, intelligent systems based on classification and learning techniques have emerged over the last years in medical imaging. In this paper, a new method is proposed to help medical experts in classifying the Left Ventricle (LV) wall motion without the need of image segmentation and through the learning of motion features by using dictionary learning techniques. Specifically the novelty of this approach lies in the extraction of new spatio-temporal descriptors and in the use of discriminative dictionary learning (DL) techniques to classify normal/abnormal LV function in cardiac MRI. Local radial spatio-temporal profiles are first extracted from bidimensional (2D) short axis (SAX) MRI images, for each anatomical segment of the LV cavity. These profiles inherently contain discriminatory in-

*Corresponding author
Email addresses: jjmantilla@gmail.com (Juan José Mantilla), paredesj@ula.ve (José Luis Paredes), jean-jacques.bellanger@univ-rennes1.fr (Jean-Jacques Bellanger), Erwan.Donal@chu-rennes.fr (Erwan Donal), christophe.leclercq@chu-rennes.fr (Christophe Leclercq), mireille.garreau@univ-rennes1.fr (Mireille Garreau)

© 2019 published by Elsevier. This manuscript is made available under the CC BY NC user license
https://creativecommons.org/licenses/by-nc/4.0/

formation that can help for cardiac motion characterization. An advantage of this approach is that these profiles are constructed from a very limited user interaction that corresponds to a number of five points in only one frame of the sequence, (without the need of LV boundaries segmentation) and by exploiting all the phases of the cardiac cycle. Two specific discriminative DL algorithms have been selected for the LV wall classification based on these profiles: Label Consistent K-SVD (LC-KSVD) and Fisher Discriminative (FD-DL). For the application of the proposed methods, cine-MR SAX images have been collected from a control group of 9 healthy subjects and from 9 patients with cardiac dyssynchrony. Radial strain curves in 2D Speckle Tracking Echocardiography (2D-STE) have been analysed for the patient group and have been used as reference truth. They allowed to label each profile as normal or abnormal. The best performance has been achieved in the Wavelet domain by the LC-KSVD algorithm with an accuracy of 84.07% in the classification of radial spatio-temporal profiles and using a leave-one-out patient cross validation. The approach has been compared with recent methods of the literature and offers a good compromise between performance, user interaction, time computing and complexity. This new method of LV classification, with minimal user interaction and based on discriminative DL has not been previously reported. It could help to improve the performance of pre-screening systems for cardiac assessment, which can affect positively the quality of the early diagnosis for heart failure patients.
Keywords: Dictionary Learning; LV cardiac motion; cardiac MRI;
spatio-temporal profiles; sparse signal classification.

---

1. Introduction

Assessment of Left Ventricular (LV) function is an important task in cardiac disease diagnosis. A common alteration of the LV function in patients with chronic Heart Failure (HF) is the intra-ventricular dyssynchrony. This mechanical issue occurs when regions of the ventricle contract at different times and is most commonly caused by a blocked bundle branch, a disorder of His

bundle branches (Hawkins et al., 2006) that disrupts ventricular activation sequence. Abnormal local LV wall motion is an early finding in multiple cardiac pathologies and its detection is of critical importance (Garcia-Fernandez et al., 2003). Cardiac Magnetic Resonance Imaging (MRI) is currently used in medical imaging for the assessment of LV function (Kirschbaum et al., 2011).

This modality allows the extraction of different parameters that characterize the ventricular function and that can be classified in two categories. The first one contains global indicators such as the stroke volume, the cardiac output, the ejection fraction and the ventricular mass. Global analysis of the cardiac dynamic in MRI is most often focused on two particular phases of the cardiac cycle, the end-diastole and end-systole phases. The second category concerns local parameters that represent the behavior of anatomical segments of the LV following the American Heart Association (AHA) 17 model representation (Cerqueira et al., 2002). These local parameters can include the regional ejection fraction, the myocardial thickening, motion, velocity and strain information.

Several MRI-based techniques or specific sequences can be employed to detect mechanical dyssynchrony and assess cardiac LV motion including myocardial tagging, phase contrast tissue velocity mapping and cardiac cine-MRI. Tagged magnetic resonance (TMR) is considered as gold standard for LV motion tracking as motion fields extracted from this modality already constitute an indicator of local function and are used to derive other indicators, such as strains (Garcia-Barnes et al., 2010; Morais et al., 2017). However, TMR sequences are not always available or of sufficient quality to use them in clinical routine while cine-MRI is the first sequence used. Several works in cine-MRI have been proposed for the automatic assessment of LV wall motion and some of them showed a good correlation between 2D speckle tracking echocardiography (2D-STE) and MRI. These works allow considering both MRI and STE data to extract qualitative and quantitative parameters for the assessment of LV wall motion.

The most relevant approaches that have been proposed for the automatic assessment of LV wall motion in cardiac cine-MRI can be classified in three

main groups: i) Landmark-based shape analysis methods that provide a statistical shape modelling of cardiac contraction (Ordas & Frangi, 2005; Huang et al., 2006; Suinesiaputra et al., 2009, 2011), ii) Methods based on image features extraction that consider the hypothesis that motion patterns of normal LV anatomical segments should be deviated away from patterns of abnormal LV segments (Lu et al., 2009; Punithakumar et al., 2013; Afshin et al., 2014), and iii) Methods based on parametric imaging-based quantification, that rely on the ability to integrate spatial and temporal information on LV wall motion in meaningful parametric images for motion abnormalities analysis (Caiani et al., 2004, 2006; El-Berbari et al., 2009). Current techniques for LV wall motion assessment often consider a preprocessing step, followed by the segmentation of the myocardium, feature extraction and classification stages. Therefore, it is challenging to find a method that could exploit all the information of the cardiac cycle and inherently dispose discriminatory information for cardiac motion characterization without the need of segmentation of the LV myocardium (that remains a time-consuming task) and with few user interaction.

A recent classification technique that is widely exploited in natural images is the Sparse Representation based Classification (SRC) (Wright et al., 2009) which involves the use of different algorithms to learn dictionaries from labeled training dataset and then use the features of the sparse decomposition of the testing signal for classification. This algorithm has achieved competitive performance on face recognition. However the performance of SRC has been improved by using discriminative dictionaries based on Dictionary Learning (DL) in which, the dictionary is inferred from a set of input signals (Rubinstein et al., 2010), such that a given signal can be well approximated by a linear combination of a few atoms in the dictionary.

Some successful applications in medical imaging, based on sparse representation and DL approaches, have been explored for image reconstruction, image denoising, image fusion, image segmentation, multimodal images enhancement and classification. In the case of classification in medical images, some works include the detection of Multiple sclerosis (MS) lesions in FLAIR MR images of

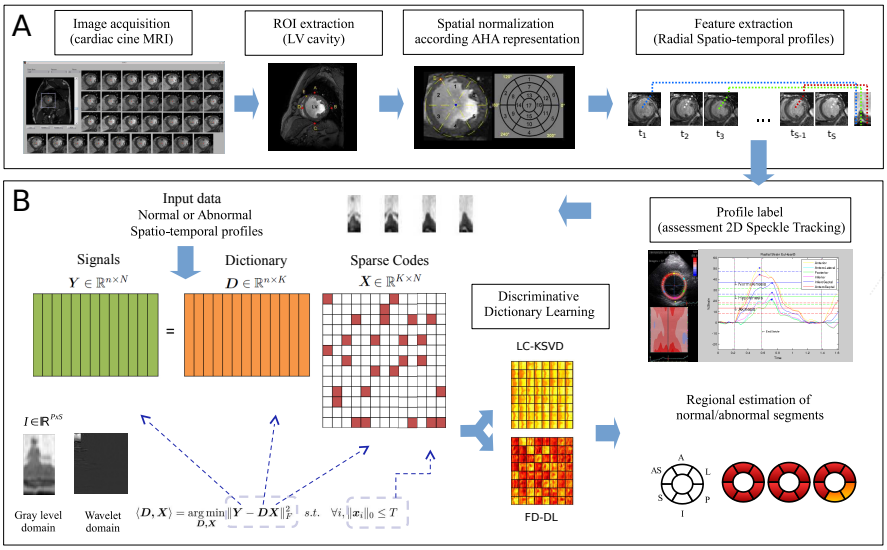


Figure 1: Overall scheme of the adaptation of discriminative DL approaches for local LV wall motion classification in cardiac cine-MRI: Top panel resumes the automated spatio-temporal images extraction steps. Bottom panel resumes the classification based on Discriminative Dictionary Learning approaches using the spatio-temporal profiles in gray level and Wavelet domains assessed by 2D-STE in the mid-cavity slice to provide in a final stage, a regional estimation of normal/abnormal segments in bull-eye representations.

the brain (Weiss et al., 2013; Deshpande et al., 2014), the classification of lung needle biopsy images (Shi et al., 2013) and the histopathological image representation and classification (Srinivas et al., 2014). In cardiac medical images, works are focused on echocardiography images for the tracking (Huang et al., 2014) and the segmentation (Rosas-Romero & Tagare, 2014) of both endocardial and epicardial contours of the LV. More recently in (Guo et al., 2015), a fully automatic classification method based on sparse representation has been proposed to distinguish intracardiac tumor and thrombi in echocardiography. To the best of our knowledge, classification of LV wall motion based on discriminative DL in cardiac MRI has not been previously reported.

In the context of Heart Failure, we aimed at developing new methods for the assessment of LV wall motion in cardiac cine-MRI that is currently used in medical imaging for the assessment of LV function. In clinical practice, this assessment relies mainly on semi-manual segmentations as well as on visual analysis and interpretation of wall motion by experts. Supplying the clinicians with semi-automatic tools (by integrating a learning process) to classify cardiac motion and with minimal user interaction remains a challenge.

In this study, a classifier is learned jointly with a dictionary, so the dictionary is designed by respecting classification constraints as well. This leads to the study of two types of discriminative dictionaries: the label consistent K-SVD algorithm (LC-KSVD) (Jiang et al., 2013) and the Fisher discriminant DL algorithm (Yang et al., 2014). A first work has been proposed in this direction in (Mantilla et al., 2013) using a simple feature extraction procedure, based only on diametrical profiles extracted from short-axis cardiac cine-MRI, and without any assessment protocol.

In this paper, we propose a novel approach based on the extraction of new spatio-temporal descriptors combined with discriminative dictionary learning techniques to obtain a binary local classification between normal and abnormal LV wall motion in cine-MRI. The innovative part of this approach is mainly concerned by the application of Dictionary Learning techniques based on Sparse Representation for Left Ventricle motion classification, and by the extraction of

spatio-temporal features in one only process, based on ROIs that are deduced from very limited user interaction (only five reference points in the first frame) with no boundaries segmentation. To this end, radial spatio-temporal profiles that describe LV's wall motion for each anatomical segment are extracted from the cine-MRI short axis images. These profiles are taken as input atoms in the training of the discriminative dictionaries for LV wall classification.

Experimental results show the improvement in the performance of cardiac motion characterization and confirm that the proposed method could be a good alternative for LV wall motion classification for clinical experts. Moreover, being fully computational and involving minimal manual steps, it is adapted and could be used as a core component within an effective expert system framework for cardiac motion characterization.

Our method differs from those methods reported in the literature in three points: 1) the feature extraction procedure which exploits all the information contained in the cardiac cycle without the need of segmentation of the epicardial and endocardial boundaries, 2) the use of DL techniques for classification of LV wall motion in cardiac MRI and 3) the evaluation method where, with the lack of a gold standard technique such as TMR, we extract strain measures from 2D-Speckle tracking Echocardiography from which the analysis of radial strain curves is performed for the assessment of the proposed spatio-temporal profiles. This process is controlled by a cardiologist and the classification is compared and validated with information obtained by physicians in cine-MRI. This technique is used as ground truth to label the proposed spatio-temporal representations. A broader discussion of the discriminative DL classification techniques is presented in terms of complexity (sparsity and computational times).

In this work, that is relevant from artificial intelligence techniques, we have demonstrated the benefits of using discriminative dictionaries, directly learned from a set of new extracted spatio-temporal descriptors, that capture the distribution of motion information in the data (without the need of segmentation) that is then used in classification tasks for normal/abnormal LV detection.

The next subsection describes the overall scheme of the proposed approach

and the organization of this paper.

2. Overall scheme of the proposed approach

An overview of the novel approach is shown in Fig. 1. A first global stage called "automated spatio-temporal images extraction" (Part A in Fig. 1) is proposed including the collection of data, a Region of Interest (ROI) extraction procedure and a new feature extraction procedure performed with the construction of radial spatio-temporal profiles overall the labeled anatomical segment spatially normalized according to the AHA representation. In a second global stage (Part B in Fig. 1), the assessment of these profiles is first performed with the analysis of the radial strain curves available from 2D Speckle Tracking Echocardiography (STE) technique. Finally, the spatio-temporal profiles considered in the original (gray level) and the Wavelet domains, are taken as input data for the training of the discriminative DL approaches. This stage allows us to obtain the results of local LV wall motion classification that are presented in the parametric bull-eyes images in the mid-cavity slice. In the next sections of this paper each step is described in detail: Section III describes the methodology that is proposed for the automatic extraction of spatio-temporal profiles from cine-MRI. Section IV presents the discriminative DL approaches that have been used for LV wall motion classification. Section V describes the experimental protocol of validation, the classification results and a study of robustness. Finally discussion and concluding remarks are presented in Sections VI and VII, respectively.

3. Automatic extraction of spatio-temporal profiles

3.1. Image acquisition

In cardiac MRI, in clinical routine, images for all cardiac phases can be acquired in cine mode using 1.5T or 3T systems. A cardiac cine-MRI sequence contains S temporal frames (usually between 25 and 40), each frame comprising R slices routinely divided in three spatial levels (or planes): basal, mid-cavity

and apical levels. A typical cardiac cine-MRI presents a temporal resolution of 30 ms, a spatial resolution of 1.5 mm (in-plane) and a slice thickness varying from 8 to 10 mm. The short axis view of any of these slices shows a cross-section of the left and right ventricles.

3.2. ROI extraction

The goal in this stage is to extract the ROI corresponding to the LV that is then retained in each frame before applying the extraction of spatio-temporal profiles. To this end, the center of the LV and the anterior intersection between the two ventricles are determined with the placement of 5 points selected manually by the user only in one reference frame at the end-diastolic phase and for each plane (basal, mid-cavity, apical). As illustrated in Fig. 2-(bottom-left), the first four points labeled as A, B, C and D located outside the epicardial border respectively in the anterior, lateral, inferior and septal wall at the end-diastolic phase, are used to calculate the LV centroid and to delimit the ROI that is assumed to contain the LV in all the sequences. We select the end-diastolic phase in each plane because in this phase the LV presents the biggest volume. The ROI that results from the five reference points is then propagated without user efforts in all the images of the sequence. The fifth point (E) is placed in the anterior intersection of the left ventricle and the right ventricle (RV) and will serve as reference in the spatial normalization step. The selection of these points in only one frame of the sequence is the only user assistance required by the overall proposed approach. This process needs some anatomical and clinical knowledge to place the anterior intersection beween RV and LV, but it is much easier than a contour delineation and very easy for the expert in very fast time.

3.3. Spatial normalization

Because of the variability inherent to the patient position in the scanner system and to the heart position in the thorax, we need to normalize different heart positions to the same reference. As illustrated in Fig. 2-(bottom-left), an axis (yellow line) crossing the anterior intersection of the two ventricles and the

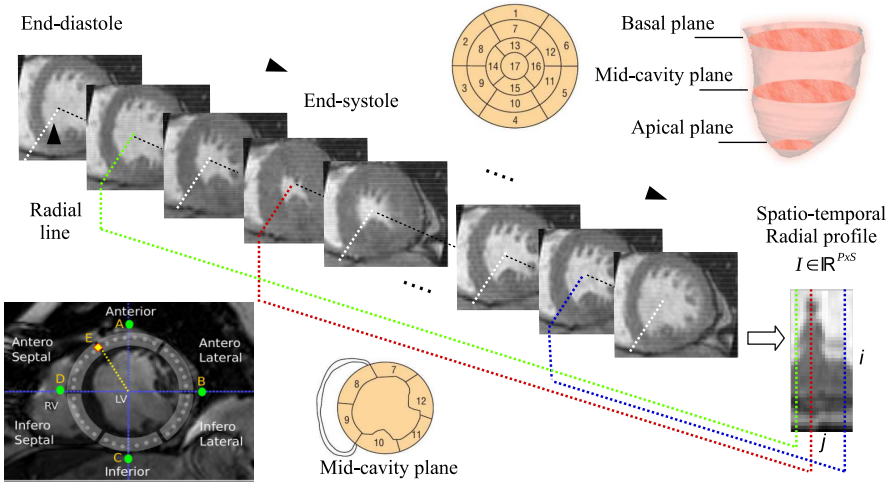


Figure 2: Process of construction of the spatio-temporal image from a radial profile in the infero-septal segment for a control patient. Each radial profile is obtained from end-diastole phase during one cardiac cycle going through the end-systole phase. In the same figure, Spatial normalization according to the AHA 17 myocardial Segments (Cerqueira et al., 2002). For the mid-cavity plane: 7, Anterior; 8, Antero-Septal; 9, Infero-Septal; 10, Inferior; 11, Infero-Lateral; 12, Antero-Lateral.

LV centroid is used as reference in order to spatially normalize the LV cavity. Heart shape variations have no influence in the definition of anatomical segments. The choice of the reference line is not dependent on the image coordinate system nor on the position of the septal wall. This procedure allows the identification of different anatomical segments according the AHA representation (Cerqueira et al., 2002), for example, in the mid-cavity plane: anterior, antero-septal, infero-septal, inferior, posterior/infero-lateral, and lateral/antero-lateral segments. Each anatomical segment is then labeled as normal or abnormal in the classification process.

3.4. Feature extraction

Figure 2 illustrates the proposed automatic process for the extraction of spatio-temporal profiles. Radial lines are traced from the LV centroid to a point outside of the epicardial border in end-diastolic view. Each line in the same orientation is then projected into the next frames of the cardiac sequence. A spatio-temporal image $I \in \mathbb{R}^{P \times S}$ (called radial spatio-temporal profile), is obtained by the concatenation of the image's gray levels along the radial line, where P denotes the length of the radial line and S represents the number of temporal frames in a cardiac cycle. For the normalization of the LV's size among patients, we have observed the length of the radial lines at the end-diastolic phase in the basal short axis plane in all the patients. We select this reference plane because at the basal plane the LV ventricle presents the bigger size. The radial line holds between 35 and 58 points for all the patients, which corresponds to approximate 43.75 and 72.5 mm as the resolution in-plane in this study corresponds to $1.25 \times 1.25\ mm^2$ per pixel.

Then we select a reference average of 40 points (radial line of 50 mm). Every spatio-temporal image is then linearly interpolated along the vertical direction (P= 40 points), while, a bicubic interpolation is then performed along the horizontal direction (S= 20 points) leading to a spatio-temporal image $I'' \in \mathbb{R}^{40 \times 20}$ (Suinesiaputra et al., 2009; Lu et al., 2009). Then, the radial spatio-temporal profiles are normalized in intensity for comparison purposes across

slices, phases and subjects. For that purpose, each pixel in each spatio-temporal image is set to $(I''_{i,j} - \mu)\ /\sigma$, where, $I''_{i,j}$ is the interpolated pixel intensity value (after spatio-temporal normalization), μ and σ are, respectively, the mean and the standard deviation of the spatio-temporal image $I'' \in \mathbb{R}^{40\times 20}$.

Finally, for each patient, a set of $I_M^R \in \mathbb{R}^{40\times 20}$ (radial normalized spatio-temporal profiles) is obtained, where $R \in \{1, 2, 3\}$, each number associated with a short axis slice level (apical, medial and basal) and $M \in \{1, \ldots, 360\}$, $\Delta\theta = 1°$, each angle θ associated with a profile orientation in the 360° scans of the LV.

From the radial spatio-temporal image $I_M^R \in \mathbb{R}^{40\times 20}$, features are extracted directly on the gray level domain (original image domain) and also in the Wavelet domain, after performing a three-level db4 2-D discrete Wavelet Transform, following the sparsifying transform used in the thresholding experiment described in (Lustig et al., 2007) obtaining a new representation $\Psi_M^R \in \mathbb{R}^{64\times 64}$.

This technique of feature extraction differs from the work of Lu (Lu et al., 2009) by the fact that features are extracted in one process in spatio-temporal dimension and that they represent the grey levels (or wavelets), providing information on displacement and motion of the myocardium, but also outside the myocardium.

4. Discriminative Dictionary Learning for classification of spatio-temporal profiles

We aim at classifying whether an anatomical segment presents LV wall motion abnormality or not, by using radial spatio-temporal profiles and by using recent discriminative DL approaches. We aim to compare our results to those obtained by using classical classification techniques based on SVM methods.

The first discriminative DL technique used for LV wall motion classification is the Label Consistent DL (LC-KSVD) algorithm (Jiang et al., 2013) (Equation 1), which presents two variants: the first one, denoted here as LC-KSVD1 takes only one structural constraint on the dictionary, that is represented by $\|\boldsymbol{Q} - \boldsymbol{AX}\|_2^2$, the discriminative sparse-code error term; the second one, named LC-

KSVD2, takes two structural constraints on the dictionary: the discriminative sparse-code error term and the classification error that is represented by $\|\boldsymbol{H} - \boldsymbol{W}\boldsymbol{X}\|_2^2$.

$$\begin{aligned} \langle \boldsymbol{D}, \boldsymbol{W}, \boldsymbol{A}, \boldsymbol{X} \rangle \quad = \quad & \underset{\boldsymbol{D},\boldsymbol{W},\boldsymbol{A},\boldsymbol{X}}{\arg\min} \|\boldsymbol{Y} - \boldsymbol{D}\boldsymbol{X}\|_2^2 + \\ & \alpha\|\boldsymbol{Q} - \boldsymbol{A}\boldsymbol{X}\|_2^2 + \beta\|\boldsymbol{H} - \boldsymbol{W}\boldsymbol{X}\|_2^2 \\ & s.t. \quad \forall i, \|\boldsymbol{x}_i\|_0 \leq T, \end{aligned} \tag{1}$$

where: $\boldsymbol{Q} = [\boldsymbol{q}_1, \ldots, \boldsymbol{q}_N] \in \mathbb{R}^{K \times N}$ are the discriminative sparse codes of the input radial spatio-temporal profiles I_M^R or Ψ_M^R vectorized as $\boldsymbol{\iota} \in \mathbb{R}^{800}$ and $\boldsymbol{\psi} \in \mathbb{R}^{4096}$ respectively, for classification and $\boldsymbol{A}$ is a linear transformation matrix. The linear transformation, $g(\boldsymbol{x}; \boldsymbol{A}) = \boldsymbol{A}\boldsymbol{x}$, transforms the original sparse codes coefficients $\boldsymbol{x}$ to be most discriminative in the sparse feature space $\mathbb{R}^K$. $\boldsymbol{W} \in \mathbb{R}^{m \times K}$ denotes the classifier parameters, where m is the number of classes ($m = 2$, normal/abnormal profiles). $\boldsymbol{H} = [\boldsymbol{h}_1, \ldots, \boldsymbol{h}_N] \in \mathbb{R}^{m \times N}$ are the class labels of input profiles $\boldsymbol{Y}$. α and β are weights, respectively for label constraint term and for classification error term.

The second discriminative DL technique that has been used for the classification of radial spatio-temporal profiles is the Fisher Discriminative DL (FD-DL) algorithm (Yang et al., 2014). This approach proposes to learn a structured dictionary $\boldsymbol{D} = \left[\boldsymbol{D}_1 \,\vdots\, \boldsymbol{D}_2\right]$, where $\boldsymbol{D}_1$ is the class-specified sub-dictionary associated with the class of abnormal profiles, and $\boldsymbol{D}_2$ is the class-specified sub-dictionary associated with the class of normal profiles. In the FD-DL algorithm, the Fisher discrimination criterion is imposed on the coding coefficients $\boldsymbol{X}$ to make them discriminative. We denote $\boldsymbol{Y} = \left[\boldsymbol{Y}_1 \,\vdots\, \boldsymbol{Y}_2\right]$ the set of training profiles (abnormal/normal respectively). Let $\boldsymbol{X}$ be the coding coefficient matrix of $\boldsymbol{Y}$ over $\boldsymbol{D}$ i.e., $\boldsymbol{X} = \left[\boldsymbol{X}_1 \,\vdots\, \boldsymbol{X}_2\right]$, where $\boldsymbol{X}_1$ and $\boldsymbol{X}_2$ are the sub-matrices containing the sparse coding coefficients of $\boldsymbol{Y}_1$ and $\boldsymbol{Y}_2$ respectively over $\boldsymbol{D}$. The dictionary $\boldsymbol{D}$ and the coding coefficient matrix $\boldsymbol{X}$ are obtained by solving:

$$\langle \boldsymbol{D}, \boldsymbol{X} \rangle = \underset{\boldsymbol{D},\boldsymbol{X}}{\arg\min} \left\{ r(\boldsymbol{Y}, \boldsymbol{D}, \boldsymbol{X}) + \lambda_1 \|\boldsymbol{X}\|_1 + \lambda_2 f(\boldsymbol{X}) \right\}, \tag{2}$$

where $r(\boldsymbol{Y}, \boldsymbol{D}, \boldsymbol{X})$ is the discriminative fidelity term, $\|\boldsymbol{X}\|_1$ is the sparsity constraint regularized by the ℓ_1-norm, $f(\boldsymbol{X})$ is a discrimination constraint imposed on the coefficient matrix $\boldsymbol{X}$ regularized by the ℓ_2-norm. λ_1 is the regularization parameter that governs the sparsity of the solution and λ_2 is a regularization parameter that enforces $\boldsymbol{X}$, to be discriminative based on the Fisher discrimination criterion. As we can see, both ℓ_1-norm and ℓ_2-norm regularizations are imposed on the representation coefficient matrix $\boldsymbol{X}$.

5. Experiments and Results

5.1. Population and Image Acquisition

The experimental procedures involving human subjects described in this paper were approved by the ethics committee of the CHU-Pontchaillou in Rennes, and were conducted in accordance with the Declaration of Helsinki. The short-axis cine-MRI databases used in these experiments were collected from three groups: two groups of data patients candidates for cardiac resynchronization therapy, that were acquired from clinical protocols in national and international research projects composed of 3 and 6 patients, respectively (group G1 and G2); and one control group (G3) formed by 9 healthy patients obtained from an online database (Tobon-Gomez et al., 2013). For the experimental part on these data, all the acquisitions were obtained with a Philips Medical System Achieva 3T MRI scanner with, 30 phases over the cardiac cycle for the first group of data patients (G1), 40 phases for the second group (G2) and 30 phases for the control group (G3). In summary, the 18 cases were identified in two classes: 1) patients with abnormal LV motion samples corresponding to 9 patients with cardiac dyssynchrony and 2) patients with normal LV motion samples that correspond to 9 healthy subjects. Data in SAX view used in these experiments did not present image shifting due to breath-hold.

For each patient in both groups (pathological and control), we disposed of 360 profiles ($\Delta\theta = 1°$), however, after performing several experiments varying the number of profiles, we found out that by selecting only 36 profiles

($\Delta\theta = 10°$), and a limited number of profiles by anatomical segment (e.g. 6 at the mid-ventricular slice level), the proposed approach achieves a good compromise between complexity and classification. To resume, results described in these experiments have been obtained from a total of 648 radial spatio temporal profiles corresponding to 18 patients x 6 anatomical segments per patient in the mid-cavity slice x 6 radial profiles per segment.

5.2. Assessment of radial spatio-temporal profiles with echocardiography 2D-STE

In the group of pathological patients, radial strain tracings from 2D-STE were available only at the mid-cavity plane. For these patients a cardiologist, expert in echocardiography, performed Trans-thoracic echocardiography TTE US acquisitions. STE traces and regional strain curves were computed and exported using an echoPAC clinical workstation software (GE). Only SAX images have been used in this work. In order to perform the evaluation of the proposed method, the experiments and results presented in this paper correspond only by considering the medial plane in MRI. Previous works have demonstrated the relation between myocardial strain and strain rate calculated from two dimensional echocardiography versus regional LV function defined by cardiac cine-MRI for the assessment of regional left ventricular function (Becker et al., 2006) and for the assessment of suitable segments for LV lead placement in cardiac resynchronization therapy (Bakos et al., 2014).

First, a spatial matching between cine-MRI slices and 2D-STE slices is needed. To solve this problem, a visual inspection supported by the medical reports of the 9 patients has been performed in order to find a correspondence between the SAX plane used in the 2D-STE study and the SAX plane selected in the cine-MRI study. This inspection is particularly, based on the visualization of the papillary muscles observed in both images. For some patients, only certain anatomical segments present abnormal movement which is in accordance with the radial strain tracings analysed from the the 2D-STE. Various studies have focused on the definition of normal values of LV motion in this modality (Becker

et al., 2006; Fine et al., 2013; Yingchoncharoen et al., 2013). Our analysis is based on reference values reported in the literature (Becker et al., 2006) shown in Table 1 that allows the classification of the profiles in the cardiac cine-MRI study as normal (normal kinesis in the STE study), or abnormal (hypokinesis or akinesis cases in the STE study). The analysis in (Becker et al., 2006) was performed with a relative variability of 8.7 ± 7.1% for the peak systolic radial strain between 2D-STE and cardiac cine-MRI. Due to the standard deviation

Table 1: Radial strain related to regional LV function defined by cardiac magnetic resonance imaging reported in (Becker et al., 2006)

	Radial Strain(%)
Normal kinesis (n=399 segments)	36.8 ± 10.5
Hypokinesis (n=392 segments)	24.1 ± 7.5
Akinesis (n=110 segments)	13.4 ± 4.8
p Value	<0.01

Table 2: Results of classification using radial profiles in mid-cavity level in Gray level and Wavelet domain by the SVM and DL models using LOO patient cross validation

	Gray level			Wavelet		
Classifier	Accuracy	Sensitivity	Specificity	Accuracy	Sensitivity	Specificity
linear	67.63 ± 27.05	86.11 ± 11.19	59.78 ± 32.71	74.32 ± 20.86	71.54 ± 33.10	66.54 ± 24.70
RBF	72.38 ± 25.45	88.88 ± 13.24	69.59 ± 33.78	69.52 ± 23.72	76.08 ± 27.44	68.20 ± 23.77
LC-KSVD 1	70.06 ± 16.54	65.83 ± 23.84	77.46 ± 9.25	82.53 ± 15.53	80.77 ± 23.88	87.16 ± 10.18
LC-KSVD 2	69.44 ± 17.25	65.83 ± 23.84	76.54 ± 9.32	84.07 ± 15.99	80.77 ± 23.88	89.62 ± 8.21
FD-DL	70.38 ± 10.53	69.31 ± 13.84	72.45 ± 12.25	83.97 ± 12.90	78.77 ± 20.81	91.62 ± 4.19

into the ranges, a peak radial strain value can fall in two overlapping zones i.e, normal kinesis or hypokinesis, thus, we select the range with the mean value closest to the peak value in study. The process has been established with the supervision of a cardiologist and the classification has been confirmed and validated with information obtained in the cine-MRI studies assessed by physicians

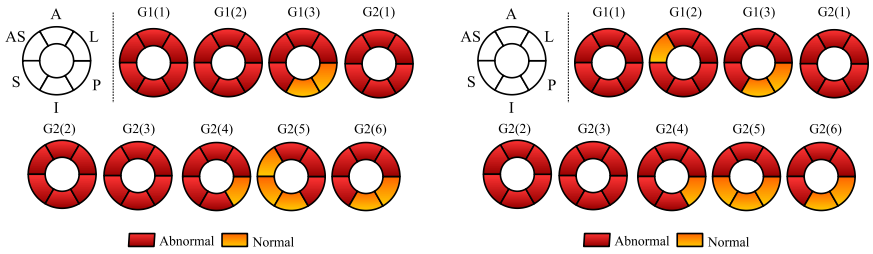


Figure 3: Ground truth for Local LV wall motion in mid-cavity level with the assessment of STE in the pathological group (left) and Local LV wall motion in the pathological group obtained by the three discriminative DL techniques for LV wall motion classification (right).

in the medical reports. In these reports visual qualitative scores were available for those segments with hypokinesis or akinesis. Also, delayed contraction between segments was observed and interpreted as abnormal regional motion. In our data, 5 of the 9 pathological patients present akinesis or hypokinesis in all segments, whereas the other 4 patients present some segments with normal kinesis. We cataloged all the 324 radial spatio-temporal profiles corresponding to the 9 control subjects as normal, assuming that all of them present normal kinesis. It corresponds to : 9 subjects x 6 anatomical segments x 6 radial profiles, that corresponds to 324 radial profiles. From the 324 profiles of pathological subjects we finally have 276 profiles cataloged as abnormal and 48 as normal. Experiment results are presented in the next sub-section, comparing the results of classification using the SVM technique with the three proposed approaches based on discriminative dictionary learning for LV wall motion classification: the LC-KSVD1, LC-KSVD2 and FD-DL algorithms.

5.3. Experimental protocol

In order to compare the generalization capability of the discriminative DL techniques to those achieved by the SVM models we have performed a leave-one-out (LOO) patient cross-validation where in each iteration, radial profiles from a single patient are used for testing data and profiles from the other patients are used for training the classifier. All the experiments have been conducted

using the profiles defined in the image domain as well as the profiles defined in the Wavelet domain. Then we quantify the results of classification in terms of accuracy, sensitivity and specificity defined, respectively as:

$$\text{Accuracy}=\frac{T_P+T_N}{P+N},\quad \text{Sensitivity}=\frac{T_P}{P},\quad \text{Specificity}=\frac{T_N}{N}$$

where T_P denotes true positives (number of correctly classified profiles as abnormal movement), and T_N denotes true negatives (number of correctly classified profiles as normal movement). The total labeled profiles with abnormal and normal movement are P and N, respectively.

5.4. Classification performance

The classifier performance is assessed with a LOO-patient cross validation criterium. In this case, the training is performed with the profiles of 17 patients and profiles from the patients left out are used to test the classifier. LOO-patient cross validation results of classification in terms of accuracy, sensitivity and specificity are presented in table 2 in the original (gray levels) and Wavelet domain respectively. Results are provided by processing a number of 648 (2x324) radial profiles in the mid-cavity level.

For the discriminative DL classification methods, an initial dictionary with many atoms as input spatio-temporal profiles for training is used. Similar results in terms of accuracy are obtained in the gray level domain for both techniques. However, the Wavelet domain is the space domain where classification is more accurate i.e., using a linear SVM with an accuracy of 74.32% and using the LC-KSVD2 with an accuracy of 84.07%. The difference between the two techniques is more notorious in terms of accuracy and specificity being around 10% and 20% respectively, much higher in the DL models than those obtained with SVM.

LOO-patient cross validation give us a meaningful interpretation of results inasmuch we can obtain information per anatomical segment and subjects. For this purpose, results are presented in parametric images known as bull-eyes (only in the mid-ventricular slice level) where segment colors are determined using the majority voting rule on radial profiles per anatomical segment. Specifically,

if more than a half of the 6 profiles examined in one anatomical segment is classified as normal, then, orange color is assigned to that segment. Red color is assigned to one segment if more than one half of the profiles is classified as abnormal. If exactly one half of the profiles is classified as normal and the other half as abnormal then a decision can not be taken. Figure 3-left shows the bull-eyes of the reference truth with the assessment of STE for the 9 pathological patients whereas Fig. 3-right, shows the bull-eyes obtained using the discriminative DL techniques that, after the majority vote strategy, have provided the same results for the three algorithms: LC-KSVD1, LC-KSVD2 and FD-DL. This is explained by the similarity of results in terms of sensitivity and specificity observed for the 3 DL techniques.

As we can see in Fig. 3-right, the discriminative DL algorithms are able to detect the normal regions in patients G1(3), G2(4) and G2(6) and fail in the identification of normal/abnormal wall motion in only one segment in the patient G1(2) (one false negative) and in two segments in the patient G2(5) (one false negative and one false positive). For the other patients all the segments have been well identified. The best LOO results using SVM reported in (Mantilla et al., 2015) have been obtained using a linear kernel. By using the bull eye representation, this technique is unable to make a decision in one segment in patients G2(2), G2(5) and G2(6) failing in the classification of normal wall motion in one segment in patient G2(6). It should be noted that the SVM models report low values of specificity resulting in the misclassification of several segments in normal subjects. Opposite to SVM methods, the discriminative DL models achieve high values of specificity leading to an accurate classification for all segments in the normal subjects.

Experiments have been performed on a PC with a 2.50GHz Intel(R) Xeon(R) processor. Computational times shown in table 3 are calculated using the optimal parameters for each algorithm and averaging over 50 trials. As we can see, SVM and LC-KSVD techniques employ less than 0.1 seconds for testing whereas FD-DL employs about 1.2 seconds which is considered acceptable for the application in study. FD-DL employs more computational time for training

than the other algorithms but it remains still fast.

Table 3: Time employed by the classification techniques in the Wavelet domain

	Learning Time (sec)	Testing time (sec)
SVM LINEAR	1.090 ± 0.155	0.004 ± 0.001
SVM RBF	1.041 ± 0.182	0.030 ± 0.004
LC-KSVD 1	7.360 ± 0.110	0.051 ± 0.034
LC-KSVD 2	7.340 ± 0.100	0.049 ± 0.001
FD-DL	51.170 ± 2.610	1.170 ± 0.420

5.5. Robustness study

To evaluate the generalization capability of the proposed approach, we take several subsets of samples from the original database. Each subset is composed of training and testing groups. Most specifically, we take randomly 75% of the radial spatio-temporal profiles cataloged as abnormal to conform one half of the training group. The other half has the same number taken randomly from the group of normal profiles. This is, an initial dictionary is composed of 414 profiles where 207 correspond to abnormal profiles (75% of the 267 abnormal profiles) and 207 to normal profiles. The rest of profiles (234 profiles, 168 normal and 66 abnormal) that are not taken in the training stage are selected to test the methods. We repeat this procedure during 50 iterations. Then, we calculate the average classification accuracy of the LC-KSVD and FD-DL algorithms by reducing the number of atoms in the initial dictionary. Figure 4 shows the effect of varying the dictionary size in the Wavelet domain for K = 5%, 10%, 25%, 50%, 75%, 90% and 100% of the original number of atoms in the dictionary for the three discriminative DL algorithms. In this figure, we can see that LC-KSVD2 maintains higher classification accuracy compared to LC-KSVD1, highlighting the importance of the classification error term ($\|\boldsymbol{H} - \boldsymbol{W}\boldsymbol{X}\|_2^2$) in the objective function of the discriminative DL model. FD-DL maintains a similar behavior as the LC-KSVD2 algorithm. Note that LC-KSVD1 is very

sensitive to the dictionary size. We have also evaluated the complexity of the

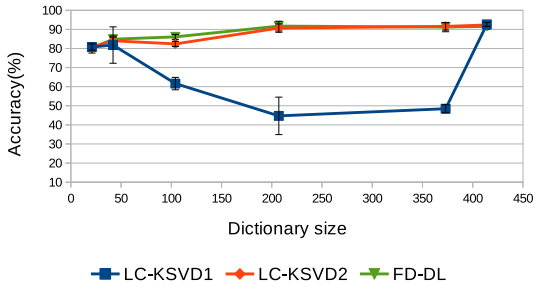


Figure 4: Accuracy of classification of the LC-KSVD and FD-DL algorithms varying the number of dictionary atoms.

classification methods in terms of sparsity. Since LC-KSVD algorithms use a ℓ_0-pseudo norm that counts the number of non-zero elements of $\boldsymbol{X}$, the sparsity constraint T can be selected as a measure of complexity in this case. We have evaluated the accuracy of the LC-KSVD algorithms for different values of the sparsity constraint T.

As results, both LC-KSVD1 and LC-KSVD2 algorithms, achieve a high classification accuracy when T is reduced, with an optimal value corresponding to 10% of sparsity. The FD-DL algorithm was evaluated in terms of ℓ_1-norm varying λ_1 that is the regularization parameter whose value governs the sparsity of the solution. The FD-DL algorithm achieves a high classification accuracy when the sparsity constraint is low, i.e., $\lambda_1 \leq 0.05$.

The regularization parameters for the machine learning techniques were tuned by heuristic search. Specifically for the linear SVM, the regularization constant (C) was varied in $[10^{-4}, 10^{-3}, 10^{-2}, 10^{-1}, 10^{0}, 10^{1}, 10^{2}, 10^{3}, 10^{4}]$ and for the SVM RBF (σ) was varied in $[0.01, 0.1, 1, 10, 100]$. For the LC-KSVD algorithms, the weight for the label constraint term (α) and the weight for the classification error term (β) were tuned by heuristic search in a mesh grid from 1 to 100 with a step of 1 unit. For FD-DL, the regularization parameters (λ_1) and (λ_2) were tuned by searching in a mesh grid from 0.01 to 10 with a step

of 0.01. This process was used for both features, in the original (image) and Wavelet domains. As results, the parameters of the machine learning techniques found as the optimal ones using 5 fold cross-validation were: for Linear SVM, $C = 100$; for RBF SVM, $C = 100$ and $\sigma = 1$. For LC-KSVD1: $\alpha = 16$, for LC-KSVD2 $\alpha = 16$ and $\beta = 4$, and finally for FD-DL: $\lambda_1 = 0.05$ and $\lambda_2 = 0.5$.

6. Discussion

Discriminative DL techniques outperform SVM models in terms of accuracy, sensitivity and specificity. The three discriminative DL techniques demand more computational time in training and testing stages than SVM, particularly the FD-DL technique. Furthermore, the difference in training and testing times between SVM and LC-KSVD techniques is very low (approximately 6 secs for training and 0.02 for testing).

The complexity of the LC-KSVD techniques in terms of sparsity can be compared with the sparseness of the SVM models. The sparseness in SVMs is measured by the number of support vectors (SV) found by the trained model. On average, the linear SVM model found 243 and 248 SVs in gray level and Wavelet domains, respectively. The RBF model found 301 and 286 SVs in the respective domains, more than 50% of the input vectors in both cases. The LC-KSVD algorithms achieve a high classification accuracy when T is reduced almost to a value of approximately 15% of the initial input atoms in the dictionary, reducing the complexity compared to the number of SVs in the SVM models. This performance is maintained even when the number of atoms is reduced in the initial dictionary e.g., by the LC-KSVD2 algorithm. Globally, in view of the results obtained, the LC-KSVD2 technique is the best compromise in terms of accuracy, sensitivity, specificity, and robustness as well as computational time i.e., in the Wavelet domain.

Related works to the assessment of LV motion in cardiac MRI based on classification techniques are summarized in Table IV. As the proposed method has been evaluated for results obtained in mid-cavity, this table represents obtained

results for this level, except for (Lu et al., 2009) that shows results only for basal slice. The degree of user interaction and the number of processed cases are also summarized.

Table 4: Comparisons of accuracy of the proposed methods with existing methods of regional LV motion classification in the mid-cavity slice

Method	Accuracy	Patients	User interaction
Proposed FD-DL	83.97	18	5 points (1 phase)
Proposed LC-KSVD1	84.07	18	5 points (1 phase)
Proposed LC-KSVD2	82.53	18	5 points (1 phase)
Proposed SVM Linear	74.32	18	5 points (1 phase)
Proposed SVM RBF	69.52	18	5 points (1 phase)
Afshin (Afshin et al., 2014)	85.72	58	Myo seg (1 phase)
Punithakumar (Punithakumar et al., 2013)	**89.40**	58	Myo seg (1 phase)
Suinesaputra (Suinesiaputra et al., 2009) (WT)	89.63	89	Myo seg (2 phases)
Suinesaputra (Suinesiaputra et al., 2009) (VWMS)	67.41	89	Myo seg (2 phases)
Lu (Lu et al., 2009) - (Basal)	86.30	17	Myo seg (N phases)

Myo seg = Manual myocardium segmentation

In these methods, the evaluation was performed by expert visual assessment. For instance, in (Lu et al., 2009) 12 of 17 patients where identified with regional abnormal wall motion for the basal slice by expert visual assessment. This method used a feature extraction procedure based on spatial profiles extracted in each frame of the cardiac cycle. The spatial profile was represented in polar coordinates by using concatenation of the gray levels of lines from the centroid to the epicardial contour previously delineated by the user. Validation was performed using an intracorrelation segment criteria. In (Afshin et al., 2014), each myocardial segment was marked following a binary score, either normal or abnormal. Starting with the delineation of the endo- and epicardial

boundaries at the first frame, the method used the Bhattacharyya measure of similarity as a statistical feature related to the proportion of blood within each segment characterizing segmental contraction. The local ground truth (per segment) was built by three experienced radiologists, each of whom annotated a different portion of the data set. Among the 928 segments identified in this study, 579 segments were marked as normal and 349 as abnormal. Results were reported using a leave-onethrid- subject-out validation criteria. In (Punithakumar et al., 2013), among the 480 myocardial segments identified in the study population, 389 segments were marked as normal and 91 as abnormal by expert visual assessment. Given the initial segmentation on the first frame, a nonrigid registration method was used to obtain sequence of points over time. From the obtained model, the Shannon differential entropy of normalized radial distance, radial velocity, segment area, segment arc length and wall thickness were evaluated for each myocardial segment. Results were reported using a leave-one-out subject validation criteria and a naive Bayesian classifier. Visual wall motion scoring for the patient group in (Suinesiaputra et al., 2009) was performed for each segment by an experienced cardiologist on a five-point scale: normokinetic, mid-hypokinetic, severe-hypokinetic, akinetic, and dyskinetic. Epi- and endocardial contours were manually drawn by an expert in the end-diastole and end-systole phases from basal, midventricular and apical levels. Results were reported using ROCs curves.

In our proposed method, a quantitative evaluation has been performed by taking information of local radial strain provided by 2D-Speckle tracking Echocardiography to label each LV anatomical segment. This process has been controlled by a cardiologist and the classification has been compared and validated with information obtained by physicians in cine-MRI. Validation was performed using both leave-one-out and random subsampling cross-validation criteria. About user interaction, in our method, only 5 manual mouse clicks are used in the first frame of the cardiac study, while other approaches seem to demand more user assistance to delineate endo and/or epicardial boundaries at least in the first frame for some methods or in all the frames for others. Only

the methods in (Afshin et al., 2014) and (Punithakumar et al., 2013) report computational times with 0.15 and 62 secs respectively. Comparative results in Table 4 show that the proposed method can yield a competitive performance while reducing the complexity and user interaction.

7. Conclusions

We have presented a new solution for local LV wall motion classification that combines: 1) a spatio-temporal feature extraction method without the need of segmentation of LV boundaries, that exploits all the information of the cardiac cycle and inherently dispose discriminatory information for cardiac motion characterization, with 2) discriminative DL techniques that achieve high capacity of generalization. To our knowledge, this is the first time that Dictionary Learning techniques based on Sparse Representation have been applied for Left Ventricle motion classification. Experiments have been performed, in the mid-cavity slice from short-axis cine-MRI. Three discriminative DL methods (LC-KSVD1, LC-KSVD2 and FD-DL) have been used and validated with information from 108 anatomical segments in a set of 18 subjects (9 patients with cardiac dyssynchrony and abnormal motion and 9 healthy subjects) from which 648 spatio-temporal profiles were extracted. Assessment of these profiles have been performed with the quantitative analysis of radial strain curves obtained from 2D STE and confirmed and validated with information of cine-MRI assessed by specialists in medical reports. DL methods have been compared with SVM models using profiles in the gray level and Wavelet domains. The best results in accuracy, sensitivity and specificity have been obtained by the DL techniques in the Wavelet domain. Local results in the mid-cavity plane have been presented in parametric images known as bull-eyes in anatomical segments of the LV according to the AHA 17 myocardial segments (only in the mid-cavity level). The complexity of the classification techniques has been compared in terms of sparseness for the SVMs and of sparsity constraint for the discriminative DL methods. The methods have been also compared in terms of computational times. We

have confirmed the use of discriminative dictionaries as an original and useful approach for the classification of normal/abnormal LV wall motion. About these approaches, We can conclude that LC-KSVD2 algorithm achieves the best compromise in accuracy (84.07%), complexity and computational times for the classification of radial spatio-temporal profiles. The performance achieved with a detailed analysis involving the proposed feature extraction method and different classifiers are important contributions for specialists interested in the study of cardiac assessment and for MRI image processing researchers, which aim to develop clinically applicable computational techniques.

By comparison with other types of recent methods, we have shown that the proposed method offers a good compromise between performance, user interaction, time computing and complexity. Along with effective applications in image processing in other fields published in the literature, dictionary learning in this paper has demonstrated its robustness in handling a complex study in cardiac MRI imaging, specifically in motion classification. This implies that the proposed approach can be implemented in real practice for analyzing MRI images, which have many useful medical applications such as diagnosis and follow-up of diseases related to heart failure.

The proposed approach shows promising results and presents several research directions for future work. For example, performance of classification of LV wall motion could potentially be improved by an expert system for automatic location of the anatomical landmark between the LV and the RV. In fact, results have shown that the classification performance has been generally improved using the different classifiers with the manual tracking of the anterior intersection between the two ventricles. The method could also be improved with an extensively validation by using more patients. We have performed a binary classification between normal/abnormal LV motion based on the spatio-temporal representations extracted in anatomical segments. This classification could be extended to a multiclass classification system into one of four classes: normal, hypokinetic, akinetic and dyskinetic LV wall motion. This work that is focused on LV wall motion characterization is planned to be extended for

characterization of cardiac dyssynchrony by considering additional parameters that could be also incorporated as input atoms in the DL-based classification methods. These parameters could include information from global functional indexes (like time-volume curves, ejection fraction, stroke volume) as well as regional anatomical and functional parameters like thickening and mechanical delays. Furthermore, this work could be extended for a new precise classification according to subgroups in Heart Failure pathologies, such as, the classification of responders or non-responders patients in the context of Cardiac Resynchronization Therapy. Further research could be the application of this work for the characterization of different cardiac pathologies and in other cardiac imaging modalities.

Acknowledgment

This work was supported in part by the French project "Utility of medical imaging for the optimization of the implantation of implantable cardiac devices" (IMOP): ANR CIC-IT n. 04 187-188-189-190, and the European project euHeart: European Community's Seventh Framework Programme FP7_ICT_2007-2(2008-12) under grant agreement n. 224495. Authors would like to thank the University of Táchira, Venezuela for the scholarship of the PhD program. Authors would also like to thank the ECOS-NORD - FONACIT grant PI-2010000299 for their financial support and Prof. Ruben Medina for the proofreading and thorough discussions. Prof. Paredes wants to thank CDCHTA-ULA for supporting his research under the project I-1336-12-02-B.

References

Afshin, M., Ben Ayed, I., Punithakumar, K., Law, M., Islam, A., Goela, A., Peters, T., & Li, S. (2014). Regional assessment of cardiac left ventricular myocardial function via MRI statistical features. *IEEE Transactions on Medical Imaging*, *33*, 481–494. doi:10.1109/TMI.2013.2287793.

Bakos, Z., Ostenfeld, E., Markstad, H., Werther-Evaldsson, A., Roijer, A., Arheden, H., Carlsson, M., & Borgquist, R. (2014). A comparison between radial strain evaluation by speckle-tracking echocardiography and cardiac magnetic resonance imaging, for assessment of suitable segments for left ventricular lead placement in cardiac resynchronization therapy. *Europace: European Pacing, Arrhythmias, and Cardiac Electrophysiology: Journal of the Working Groups on Cardiac Pacing, Arrhythmias, and Cardiac Cellular Electrophysiology of the European Society of Cardiology*, *16*, 1779–1786.

Becker, M., Bilke, E., Kuhl, H., Katoh, M., Kramann, R., Franke, A., Bucker, A., Hanrath, P., & Hoffmann, R. (2006). Analysis of myocardial deformation based on pixel tracking in two dimensional echocardiographic images enables quantitative assessment of regional left ventricular function. *Heart*, *92*, 1102–1108. doi:10.1136/hrt.2005.077107.

Caiani, E. G., Toledo, E., MacEneaney, P., Bardo, D., Cerutti, S., Lang, R. M., & Mor-Avi, V. (2006). Automated interpretation of regional left ventricular wall motion from cardiac magnetic resonance images. *Journal of Cardiovascular Magnetic Resonance*, *8*, 427–433. doi:10.1080/10976640600599486.

Caiani, E. G., Toledo, E., MacEneaney, P., Collins, K. A., Lang, R. M., & Mor-Avi, V. (2004). The role of still-frame parametric imaging in magnetic resonance assessment of left ventricular wall motion by non-cardiologists. *J Cardiovasc Magn Reson*, *6*, 619–25.

Cerqueira, M. D., Weissman, N. J., Dilsizian, V., Jacobs, A. K., Kaul, S., Laskey, W. K., Pennell, D. J., Rumberger, J. A., Ryan, T., Verani, M. S., & American Heart Association Writing Group on Myocardial Segmentation and Registration for Cardiac Imaging (2002). Standardized myocardial segmentation and nomenclature for tomographic imaging of the heart: A statement for healthcare professionals from the cardiac imaging committee of the council on clinical cardiology of the american heart association. *Circulation*, *105*, 539–542. doi:10.1161/hc0402.102975.

Deshpande, H., Maurel, P., & Barillot, C. (2014). Detection of Multiple Sclerosis Lesions using Sparse Representations and Dictionary Learning. In *2nd International Workshop on Sparsity Techniques in Medical Imaging (STMI), MICCAI 2014* 71-79. Boston, MA, United States.

El-Berbari, R., Kachenoura, N., Redheuil, A., Giron, A., Mousseaux, E., Herment, A., Bloch, I., & Frouin, F. (2009). Automated estimation of regional mean transition times and radial velocities from cine magnetic resonance images: evaluation in normal subjects. *J Magn Reson Imaging*, *30*, 236–242.

Fine, N. M., Shah, A. A., Han, I.-Y., Yu, Y., Hsiao, J.-F., Koshino, Y., Saleh, H. K., Miller, J., Fletcher A, Oh, J. K., Pellikka, P. A., & Villarraga, H. R. (2013). Left and right ventricular strain and strain rate measurement in normal adults using velocity vector imaging: an assessment of reference values and intersystem agreement. *Int J Cardiovasc Imaging*, *29*, 571–580. doi:10.1007/s10554-012-0120-7.

Garcia-Barnes, J., Gil, D., Badiella, L., Hernàndez-Sabaté, A., Carreras, F., Pujadas, S., & Martí, E. (2010). A normalized framework for the design of feature spaces assessing the left ventricular function. *IEEE Trans. Med. Imaging*, *29*, 733–745.

Garcia-Fernandez, M. A., Bermejo, J., Perez-David, E., Lopez-Fernandez, T., Ledesma, M. J., Caso, P., Malpica, N., Santos, A., Moreno, M., & Desco, M. (2003). New techniques for the assessment of regional left ventricular wall motion. *Echocardiography (Mount Kisco, N.Y.)*, *20*, 659–672.

Guo, Y., Wang, Y., Kong, D., & Shu, X. (2015). Automatic Classification of Intracardiac Tumor and Thrombi in Echocardiography Based on Sparse Representation. *IEEE Journal of Biomedical and Health Informatics*, *19*, 601–611. doi:10.1109/JBHI.2014.2313132.

Hawkins, N. M., Petrie, M. C., MacDonald, M. R., Hogg, K. J., & McMurray, J. J. V. (2006). Selecting patients for cardiac resynchronization therapy:

electrical or mechanical dyssynchrony? *European Heart Journal*, *27*, 1270–1281. doi:10.1093/eurheartj/ehi826.

Huang, H., Shen, L., Zhang, R., Makedon, F., Hettleman, B., & Pearlman, J. (2006). Cardiac motion analysis to improve pacing site selection in CRT. *J. Acad. Radiol.*, *13*, 1124 – 1134. doi:10.1016/j.acra.2006.07.010.

Huang, X., Dione, D. P., Compas, C. B., Papademetris, X., Lin, B. A., Bregasi, A., Sinusas, A. J., Staib, L. H., & Duncan, J. S. (2014). Contour tracking in echocardiographic sequences via sparse representation and dictionary learning. *Medical Image Analysis*, *18*, 253–271. doi:10.1016/j.media.2013.10.012.

Jiang, Z., Lin, Z., & Davis, L. S. (2013). Label Consistent K-SVD: Learning a Discriminative Dictionary for Recognition. *IEEE Transactions on Pattern Analysis and Machine Intelligence*, *35*, 2651–2664. doi:10.1109/TPAMI.2013.88.

Kirschbaum, S. W., de Feyter, P. J., & van Geuns, R.-J. M. (2011). Cardiac magnetic resonance imaging in stable ischaemic heart disease. *Netherlands Heart Journal*, *19*, 229–235. doi:10.1007/s12471-011-0106-4.

Lu, Y., Radau, P., Connelly, K., Dick, A., & Wright, G. (2009). Pattern recognition of abnormal left ventricle wall motion in cardiac MR. In *Proceedings of the 12th International Conference on Medical Image Computing and Computer-Assisted Intervention: Part II* MICCAI '09 (pp. 750–758). Berlin, Heidelberg: Springer-Verlag. doi:10.1007/978-3-642-04271-3_91.

Lustig, M., Donoho, D., & Pauly, J. M. (2007). Sparse MRI: The application of compressed sensing for rapid MR imaging. *Magnetic Resonance in Medicine*, *58*, 1182–1195. doi:10.1002/mrm.21391.

Mantilla, J., Garreau, M., Bellanger, J.-J., & Paredes, J. L. (2013). Machine Learning Techniques for LV Wall Motion Classification Based on Spatio-temporal Profiles from Cardiac Cine MRI. In *2013 12th International Confer-*

ence on Machine Learning and Applications (ICMLA) (pp. 167–172). IEEE volume 1. doi:10.1109/ICMLA.2013.36.

Mantilla, J., Garreau, M., Bellanger, J.-J., & Paredes, J. L. (2015). SVM-based classification of LV wall motion in cardiac MRI with the assessment of STE. In *Proc. SPIE, 10th International Symposium on Medical Information Processing and Analysis* (pp. 92870N–92870N–6). volume 9287.

Morais, P., Queirs, S., Heyde, B., Engvall, J., D hooge, J., & Vilaa, J. L. (2017). Fully automatic left ventricular myocardial strain estimation in 2d short-axis tagged magnetic resonance imaging. *Physics in Medicine & Biology*, *62*, 6899. doi:10.1088/1361-6560/aa7dc2.

Ordas, S., & Frangi, A. (2005). Automatic quantitative analysis of myocardial wall motion and thickening from long-and short-axis cine MRI studies. *Conf Proc IEEE Eng Med Biol Soc*, *7*, 7028–31.

Punithakumar, K., Ben Ayed, I., Islam, A., Goela, A., Ross, I. G., Chong, J., & Li, S. (2013). Regional heart motion abnormality detection: An information theoretic approach. *Medical Image Analysis*, *17*, 311–324. doi:10.1016/j.media.2012.11.007.

Rosas-Romero, R., & Tagare, H. D. (2014). Segmentation of endocardium in ultrasound images based on sparse representation over learned redundant dictionaries. *Engineering Applications of Artificial Intelligence*, *29*, 201–210. doi:10.1016/j.engappai.2013.09.008.

Rubinstein, R., Bruckstein, A., & Elad, M. (2010). Dictionaries for sparse representation modeling. *Proceedings of the IEEE*, *98*, 1045–1057. doi:10.1109/JPROC.2010.2040551.

Shi, Y., Gao, Y., Yang, Y., Zhang, Y., & Wang, D. (2013). Multimodal sparse representation-based classification for lung needle biopsy images. *IEEE Transactions on Biomedical Engineering*, *60*, 2675–2685. doi:10.1109/TBME.2013.2262099.

Srinivas, U., Mousavi, H., Monga, V., Hattel, A., & Jayarao, B. (2014). Simultaneous Sparsity Model for Histopathological Image Representation and Classification. *IEEE Transactions on Medical Imaging*, *33*, 1163–1179. doi:10.1109/TMI.2014.2306173.

Suinesiaputra, A., Frangi, A., Kaandorp, T., Lamb, H., Bax, J., Reiber, J., & Lelieveldt, B. (2009). Automated detection of regional wall motion abnormalities based on a statistical model applied to multislice short-axis cardiac MR images. *IEEE Transactions on Medical Imaging*, *28*, 595–607. doi:10.1109/TMI.2008.2008966.

Suinesiaputra, A., Frangi, A. F., Kaandorp, T. A. M., Lamb, H. J., Bax, J. J., Reiber, J. H. C., & Lelieveldt, B. P. F. (2011). Automated regional wall motion abnormality detection by combining rest and stress cardiac MRI: correlation with contrast-enhanced MRI. *Journal of magnetic resonance imaging: JMRI*, *34*, 270–278. doi:10.1002/jmri.22601.

Tobon-Gomez, C., De Craene, M., McLeod, K., Tautz, L., Shi, W., Hennemuth, A., Prakosa, A., Wang, H., Carr-White, G., Kapetanakis, S., Lutz, A., Rasche, V., Schaeffter, T., Butakoff, C., Friman, O., Mansi, T., Sermesant, M., Zhuang, X., Ourselin, S., Peitgen, H.-O., Pennec, X., Razavi, R., Rueckert, D., Frangi, A. F., & Rhode, K. S. (2013). Benchmarking framework for myocardial tracking and deformation algorithms: An open access database. *Medical Image Analysis*, *17*, 632–648.

Weiss, N., Rueckert, D., & Rao, A. (2013). Multiple Sclerosis Lesion Segmentation Using Dictionary Learning and Sparse Coding. In K. Mori, I. Sakuma, Y. Sato, C. Barillot, & N. Navab (Eds.), *Medical Image Computing and Computer-Assisted Intervention MICCAI 2013* number 8149 in Lecture Notes in Computer Science (pp. 735–742). Springer Berlin Heidelberg.

Wright, J., Yang, A., Ganesh, A., Sastry, S., & Ma, Y. (2009). Robust Face Recognition via Sparse Representation. *IEEE Transactions on Pattern Analysis and Machine Intelligence*, *31*, 210–227. doi:10.1109/TPAMI.2008.79.

Yang, M., Zhang, L., Feng, X., & Zhang, D. (2014). Sparse representation based fisher discrimination dictionary learning for image classification. *International Journal of Computer Vision*, *109*, 209–232. doi:10.1007/s11263-014-0722-8.

Yingchoncharoen, T., Agarwal, S., Popovi, Z. B., & Marwick, T. H. (2013). Normal ranges of left ventricular strain: A meta-analysis. *Journal of the American Society of Echocardiography*, *26*, 185–191. doi:10.1016/j.echo.2012.10.008.